Contents lists available at ScienceDirect

International Journal of Heat and Mass Transfer

journal homepage: www.elsevier.com/locate/hmt



Thermal conductivity of a Jurkat cell measured by a transient laser point heating method



R. Shrestha^a, R. Atluri^a, D.P. Simmons^a, D.S. Kim^b, T.Y. Choi^{a,*}

- ^a Department of Mechanical and Energy Engineering, University of North Texas, Denton, TX, USA
- ^b Department of Mechanical Engineering, POSTECH, Pohang, South Korea

ARTICLE INFO

Article history: Received 23 December 2019 Revised 8 June 2020 Accepted 1 July 2020 Available online 16 July 2020

Keywords: Laser point heating Thermal sensor Thermal conductivity Jurkat cell

ABSTRACT

To understand and quantify the thermal energy transfer in a biological cell, the measurement of thermal properties at a cellular level is emerging as great importance. We report herein a unique technique that utilizes a laser point heat source for temporal temperature rise in a micro-pipette thermal sensor; this technique characterizes heat conduction of a measured sample, the Jurkat cell, thus measuring the sample's thermal conductivity (TC). To this end, we incorporated the computational model in COMSOL to solve for the transient temperature and used the multi-parameter fitting of the experimental data using MATLAB. To address the influence of a Jurkat cell's chemical composition on TC, we compared three structural models for prediction of effective thermal conductivity in heterogeneous materials thereby determining the weight percentage of the Jurkat cell. When considering water and protein as the major constituents, we found that a combination of Maxwell-Euken and Effective Medium Theory modeling provides the closest approximation to published weight percent data and, therefore, is recommended for prediction of the cell composition. We validate the accuracy of the measurement technique, itself, by measuring polyethylene microspheres and observed 1% deviation from published data. The unique technique was determined to be mechanically non-invasive, capable of maintaining viable cells, and capable of measuring the thermal conductivity of a Jurkat cell, which was demonstrated to be 0.538 $W/(m \cdot K) \pm 1\%$.

 $\ensuremath{\mathbb{C}}$ 2020 Elsevier Ltd. All rights reserved.

1. Introduction

The thermal conductivity of a material is the fundamental property that governs every heat transfer problem in engineering and basic science research. With the rapid development of technology, the heat transfer in nanostructures, wires, and macromolecules has lately received intensive attention [1-3]. As an example, the superior thermal conductivity of graphene and carbon nanotubes [4,5] has raised the prospect of their application in thermal devices. Similarly, to understand a biological reaction in living cells and transport of thermal energy in biological systems, measurement of temperature and thermal properties is important. Biological reactions regulate cellular functions via exothermic and endothermic processes [6,7], and therefore the energy analysis of a cell from a thermodynamic perspective is useful. In clinical studies, cellular level temperature change and the thermal properties of the cell can be used as a unique biomarker for the detection of disease [8-11], such as early-stage cancer. Heating of cells or tissues during

thermal therapies, such as hyperthermia or thermal ablation [12], is another example that requires accurate measurement of temperature at the cellular level. Thus, the thermal characterization of cells is vital to obtain critical knowledge for screening, diagnostics, basic and clinical science, and the pharmaceutical industry.

Several thermal-analysis techniques, such as Differential Scanning Calorimetry (DSC), Micro Electro Mechanical Systems (MEMS), Scanning Thermal Microscopy (SThM), Laser Point Heating Thermometry (LPHT), self-heated thermistor and transient hot-wire technique, have been developed for measuring the thermodynamic and thermophysical properties of biological samples [12-16]. However, temperature change within the cells is usually small. Moreover, such temperature change is transient due to the thermo-influence by the extracellular environment, making temperature change difficult to measure using conventional temperature detection methods [17,18]. Commercially available thermocouple (25 μ m) [14] exists for measuring microfluidic samples [19,20]. However, when a large-sized thermocouple is used in the transient temperature measurement, the majority of the heat is consumed by the sensor itself; this is because thermal penetration depth $(\delta) \sim \sqrt{(\alpha t)}$ (α : thermal diffusivity, t: characteristic time) is

^{*} Corresponding author.

E-mail address: tae-youl.choi@unt.edu (T.Y. Choi).

very small compared to the sensor size. Some published work includes self-heated thermistor and transient hot-wire technique for measuring thermal conductivity and diffusivity of biomaterials at the tissue level [12,21]. Again, the accuracy of reported results in this tissue-level method comes into question due to sensor size. Yet the body of literature for measurement of transient temperature remains sparse on the development of micro-thermocouple sensors of size 2 μm to 20 μm [18,19]. Thus, a more precise and faster-response technique is required to measure intracellular transient temperature changes in real-time. Such designed performance measurements in technique can benefit our understanding of heat generation and heat diffusion during complex cellular activities and thus advance research in clinical diagnosis and inform therapeutic evaluations.

Conventional measurement technologies including magnetic resonance imaging (MRI), IR thermography, and Raman spectroscopy [4,22–23] provide temperature measurement capabilities. However, the spatial and/or temperature resolutions are limited in these technologies (for example MRI provides spatial and temperature resolution of 1 mm and 1 °C, respectively). The temperature sensing in this paper has superior spatial resolution compared to existing methods such as MRI [23] and infrared (IR) imaging [22]. This micropipette thermal sensor described herein can measure thermal properties, in contrast, the conventional methods (e.g., MRI, IR, fluorescence methods) can measure only temperature. The fluorescence method has an inherent limitation in accuracy of temperature measurement due to the dependence of temperature on pH [24,25]. Although cellular or subcellular resolution temperature measurements using quantum dots or fluorescent nanogels have been proposed recently [26-30], these methods are not applicable to discovery of thermal properties.

In this paper, we have developed a technique that uses a micropipette thermal sensor (MPTS) composed of a sensor tip diameter of 1.6 μm and Tin alloy-Nickel metal as the thermocouple junction; we have reported this MPTS capable of measuring the temporal temperature of a spherical sample during short pulse laser heating [31–33]. The thermal properties of the spherical sample are then determined by the multiparameter fitting of the experimental data with the temporal temperature determined from COMSOL simulation together with MATLAB. We termed this the MPTS technique, named after the micropipette thermal sensor, used in this research. To show that the MPTS technique can be used to measure the thermal conductivity of a spherical cell, polyethylene microspheres of different sizes are first tested. Then the MPTS technique is used to determine the thermal conductivity of the Jurkat cell, a nonadherent suspension cell in culture. With the successful demonstration of the MPTS technique, we intend to show that this technique can be used for in vitro applications to measure the thermal properties of live individual cells suspended in culture media. We demonstrate that the MPTS technique can be a potential tool to characterize micro size particles and viable single biological cells.

2. Theoretical background

The proposed characterization method is based on transient heat diffusion with a laser point heat source [14] for an infinite solid. The sensor is fabricated in our laboratory by creating a thermocouple junction with Tin alloy filled in a borosilicate glass pipette and Nickel thin film coated outside by sputtering [31–33]. The irradiated laser heats the sensor tip and the uniform temperature at the tip is assumed due to the superior thermal conductivity of the sensor material compared to the surrounding fluid/sample. The rise in temperature of the sensor tip during the laser irradiation is dependent on the heat diffused by conduction into the sample. The calculated heat loss due to convection through the sensor

to the surrounding fluid is negligible for the short duration of heating (500 μ s).

2.1. Numerical analysis: COMSOL multiphysics simulation

It is an analytical challenge to solve for the temperature of a time-dependent heat transfer problem, such as in this research, which consists of materials with different thermal properties, boundary conditions, and complex geometries of the sensor, the sample, and the reagent preparation substrate. In the case of the sensor, a candidate analytical solution for the transient temperature, due to the instantaneous point heat source that generates heat at a point, can be the estimation proposed by Carslaw and Jaeger [34]. However, due to the higher thermal conductivity of the sensor material than the sample, heat conduction will occur along the sensor length; this problem occurrence must then be taken into consideration for accurate analysis of heat transfer. To solve this transient heat transfer problem, a numerical solution using commercially available software, such as COMSOL Multiphysics that utilizes the finite element analysis, is used.

To solve the transient response, COMSOL uses the following governing equation.

$$\rho c_p \frac{\partial T}{\partial t} + \nabla \cdot (-k \nabla T) = Q \tag{1}$$

where ρ is the density of the material, c_p is specific heat capacity, T is temperature, t is time, k is the thermal conductivity of material and Q is heat generation.

A comparison study was conducted for the analytical and numerical solution to observe the effect of heat loss through the sensor leg. A simple model that consists of the MPTS in water, with a heat source at the tip of the MPTS was created in COMSOL and solved for the temporal temperature during the heat diffusion. Next, the analytical solution for the temperature rise at a point caused by the instantaneous point heat source was solved using MATLAB. Upon comparison, it was observed that the heat loss through the sensor significantly affects the temperature rise of the sensor. Details of the analytical and numerical analysis are reported in our previously published paper [31]. These results demonstrated the requirement to perform numerical analysis to acquire an accurate solution to the transient temperature and thus determine the thermal properties of the sample.

Therefore, we used COMSOL Multiphysics combined with MAT-LAB program. This permits us to fit the temporal temperature obtained from the simulation model to the temperature data collected from the experiment. The transient temperature data in the experiment was normalized so that it becomes a function of the thermal properties of the test sample only. Then the thermal properties of the fluid can be determined by employing the multiparameter fitting algorithm, which has the objective to minimize the difference function F between the experimental temperature (\mathcal{O}^{exp}) and temperature predicted by the simulation (\mathcal{O}^{sim}) .

$$F(k,q,r) = \sum_{n=1}^{N} \left(\emptyset_n^{Sim} - \emptyset_n^{Exp} \right)^2$$
 (2)

The thermal conductivity (k), the incident power (q) at the sensor tip and the radial distance (r) from the heat source, where the temperature rise is calculated, are the control fitting parameters for optimization used in this research. Although density and specific heat are also parameters that need to be considered for heat diffusion, we used the measured value to reduce the computation time. The values that best fit the simulation result with the experimental data are optimal values when the sum squared error (SSE) expressed by Eq. (2) is minimized.

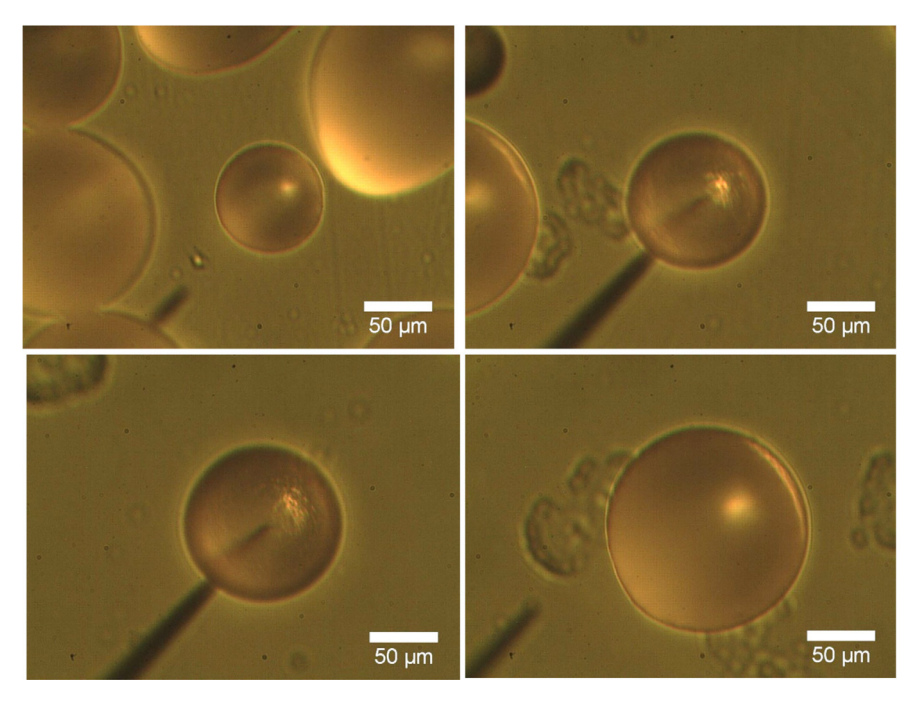


Fig. 1. Four different sizes of microspheres used for the experiment and size measured using Image].

3. Materials and method

3.1. Polyethylene microspheres

For measuring the thermal conductivity of the Jurkat cell, we first selected low thermal conductivity transparent polyethylene microspheres as a test model to validate the measurement technique. Clear polyethylene microsphere purchased from Cospheric had a size varying from 10 to 150 μm , density 0.96–0.98 g/cc and thermal conductivity of 0.33 W/(m·K). The microspheres purchased were screened to be greater than 90% in specified particle size range with greater than 90% of particles being spherical, without dust or debris and high-quality identical spheres suitable for research purpose. Microspheres were supplied in dry powder form. In the experiment, microspheres were dispersed on the glass slide and sizes were determined using ImageJ software as shown in Fig. 1.

3.2. Jurkat Cell

The acute T leukemia cell line Jurkat, Clone E6-1 (ATCC® TIB-152TM) is a non-adherent, clonal population suspension cell line. Jurkat cells were cultured in complete growth medium (GM) containing Roswell Park Memorial Institute medium (RPMI 1640 without phenol red; Gibco), with 10% Fetal Bovine Serum (FBS; Gibco) in T75 cell culture flask (Midsci) at 37 °C and 5% CO $_2$. The Jurkat cells were seeded at a concentration of 1 \times 10 5 cells/ml and maintained up to a concentration of 2 \times 10 6 cells/ml by replacing the GM every 2–3 days depending on cell density. Cultures were not used beyond Passage 7. The cells in doubling phase of growth curve at a cell density of 5.30 \times 10 5 cells/ml were used for the experiments and the average cell size, 10.5 \pm 1.6 μ m, was determined by measuring the cells using the microscope and Image] software.

3.3. PolyHydroxoEthylaMethAcrylate (polyHEMA) substrate surface preparation

As the Jurkat cells are suspension cells, they do not adhere to the surface of culture flask/ petri dish making it difficult to trap an

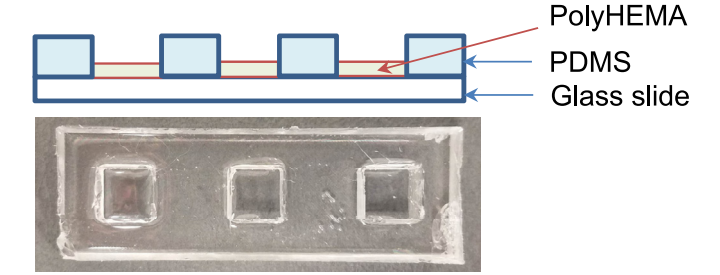


Fig. 2. PolyHEMA surface preparation on a glass slide confined by the PDMS chamber.

individual cell between the thermal sensor and dish during the experiment. Therefore, the method used for 3D culture [35] in which polyHEMA-coated plastics were used to grow cells on the surface, was used to improve cell capture on the polyHEMA gel surface. The polyHEMA (Sigma Aldrich) hydrogel was prepared in a sterile Falcon centrifuge tube by dissolving 5% weight by volume polyHEMA granules. The polyHEMA granules were mixed with 95% ethanol and kept overnight at 37 °C with gentle agitation using a magnetic stirrer. The solution was filtered, then poured on the square chambers (~ 10 mm square X 5 mm deep); chambers were prepared from polydimethylsiloxane (PDMS, Dow Corning Sylgard 184) on 75×25 mm microscope glass slide (Fisher Scientific) [36,37]. The solution was left to dry at ambient temperature, to create a thin layer (~100 µm) of polyHEMA as shown in Fig. 2. For the experiment, the chamber to be used in the experiment was rinsed with ethanol, treated with ultraviolet (UV) at a wavelength of 254 nm for 20 min and dried inside the clean laminar flow hood to prevent contamination of the cells. The Jurkat cell suspension (30-50 µl) was added to the polyHEMA layer, immediately before the experiments, and the cells were left to set on the layer for 5 min.

3.4. Experiment setup

A diode-pumped solid-state (Opto Engine LLC) laser source was used to produce a green laser (532 nm) as a point heating

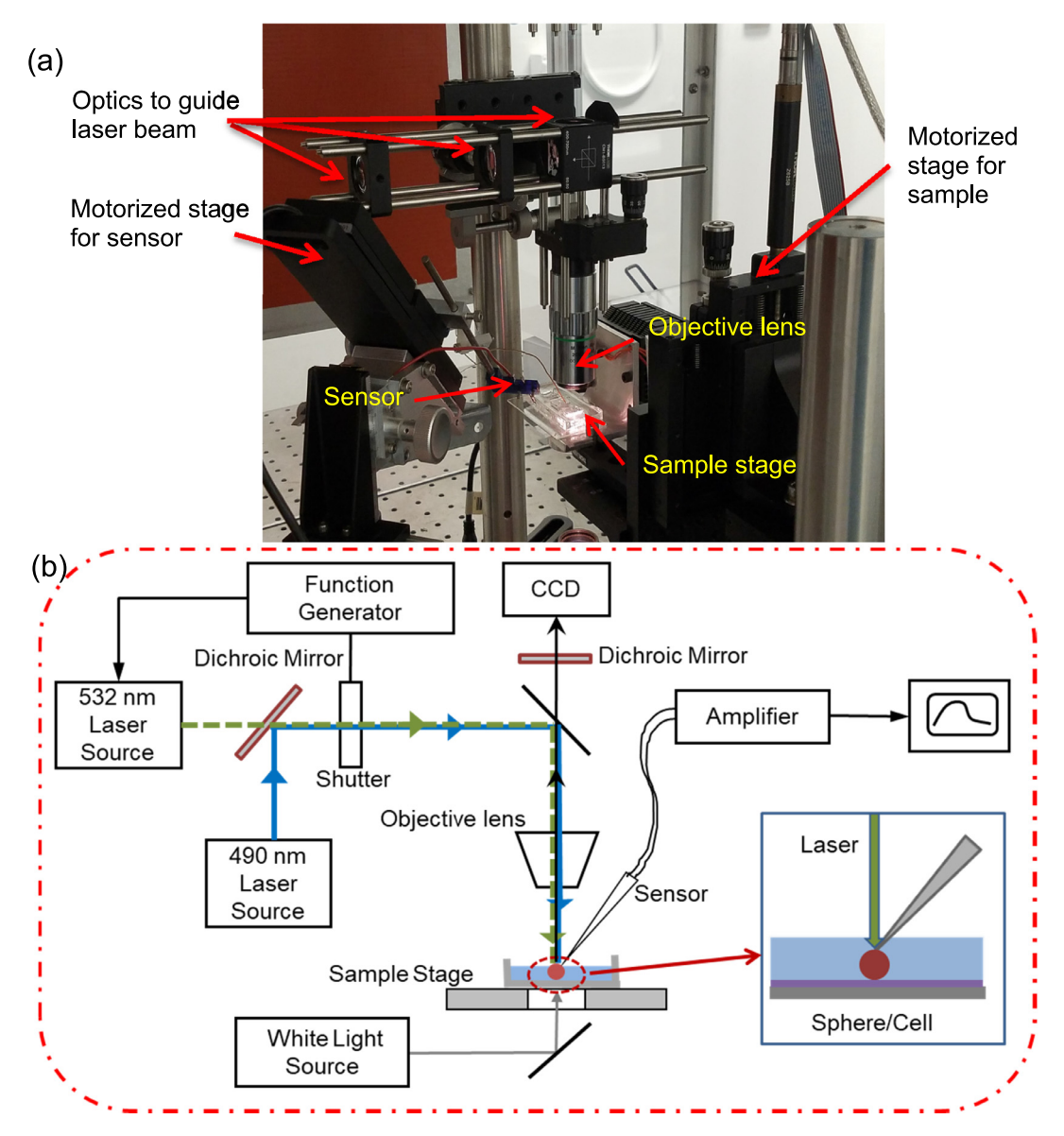


Fig. 3. (a) Picture of the experimental setup and (b) schematic of the components of the experimental setup for transient temperature and fluorescence microscopy.

source. The optics comprising shutter, mirrors, convex lens and long-distance objective lens (Mitutoyo MPlan Apo SL 20X) were arranged on the optic table as follows: a laser beam with a spot diameter of approximately 6 µm was focused on 1.6 µm diameter tip of micropipette thermal sensor with sensitivity of 8.46–8.86 μV/°C [33]. The laser power was measured using the power meter (Thor-LABS) and beam size was estimated from the image calibration. To capture the real-time image during the positioning of the sensor on the sample, a CMOS USB camera (Mightex) was used and a computer-controlled motorized stage (MTS50/M-Z8, ThorLABS) with a spatial resolution of 50 nm and repeatability of 0.8 µm was used to manipulate the sensor precisely on the sample and the beam path. Since the objective of the research was to produce a non-invasive characterization method, both positioning of the sensor onto the cell surface, rather than within the cell, as well as the use of a low dose of the laser are critical. These objective requirements set two condition goals: the intensity of laser varied such that the peak temperature rise in the sensor tip was less than 2 °C during the pulse in order not to affect the cell viability and the laser pulse of 500 µs was produced using a function generator (Agilent 33220A) and a mechanical shutter (electronically controlled by the function generator). To capture small temporal temperature changes, the voltage signals from the sensor were amplified 500 times with pre-amplifier (Stanford Research Systems SR560) and the temporal temperature for the test sample was recorded using the oscilloscope (Tektronix-TDS 2024). The schematic of the experimental setup is shown in Fig. 3.

3.5. Preparation for cell viability test

For the cell viability test of the Jurkat cell, a lab-built environment chamber, that enclosed all the equipment and the sensors, and that could circulate clean air was fabricated. Further, to check the cell viability at the beginning and the end of the experiment, an optical setup was incorporated into the main experimental setup for fluorescence microscopy. A blue laser source (490 nm) was used for excitation from top of the sample and emission (green light 532 nm) from the viable cell was captured in the camera (CCD) as a reflection. A dichroic mirror was used below the camera to prevent capturing any excitation light due to reflection.

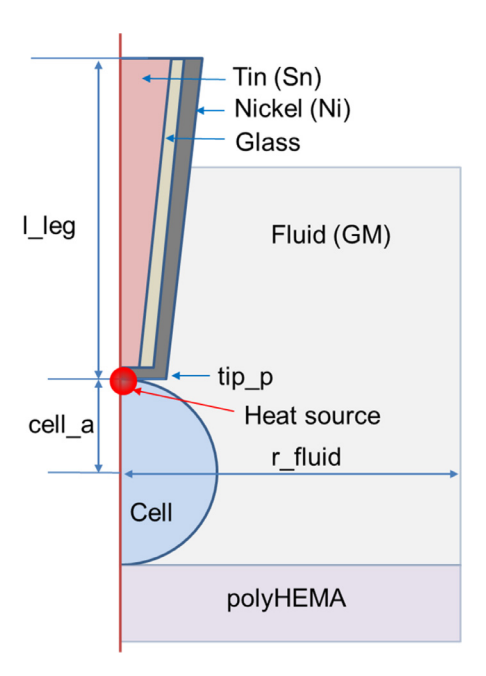


Fig. 4. A 2D axisymmetric geometry (not to scale) showing the sensor, cell/ microsphere, GM and polyHEMA used for COMSOL simulation.

A fluorescent dye stock with a concentration of 1 milliMolar (mM) was prepared using Calcein, AM (AAT Bioquest). Live/viable cells employ esterase to hydrolyze the calcein and convert the non-fluorescent calcein to a green fluorescent calcein. For the fluorescence imaging, the required volume of calcein for 10 μ M concentration needed for 10^5 cells was calculated [38] and pipetted to the desired volume of cell suspension. The calcein-AM cell suspension was incubated for 30 min at 37 °C. Then the fluorescence image was captured at three-time points: the beginning of the experiment, the end of the experiment, which was concluded within 5 min, and 15 min after the end of the experiment.

3.6. Computational model for microsphere and jurkat cell

COMSOL Multiphysics software was used for the numerical solution to the temperature change in the polyethylene microsphere and Jurkat cell touched by a heated micropipette sensor tip. A 2Daxisymmetric space dimension was chosen with an axis of symmetry slicing the sensor, cell/microsphere, fluid (growth medium GM) and substrate (polyHEMA) into half as shown in Fig. 4. Among the different dimensions captured and used in the simulation as parameters are geometry, properties values, power. The tapered section of the thermal sensor was created using the length of 200 µm, the taper angle of 5° and the tip radius of 0.81 µm determined by measurement from the microscope. The dimensions for the fluid domain and the polyHEMA substrate were selected to have a negligible boundary effect as in the case of the experiment. The laser heat source with a beam radius of 3 µm and power of 100 µW was defined at the intersection of the axis of symmetry and the sensor tip.

For the simulation, the material properties for sensor material (tin, nickel, glass) were used from the material library, while the thermal conductivity for GM and polyHEMA were determined experimentally [31]. Other properties such as specific heat capacity, density were either cited from the literature [39] or measured by weighing the specified volume for density, and determined by measuring with a differential scanning calorimeter for specific heat.

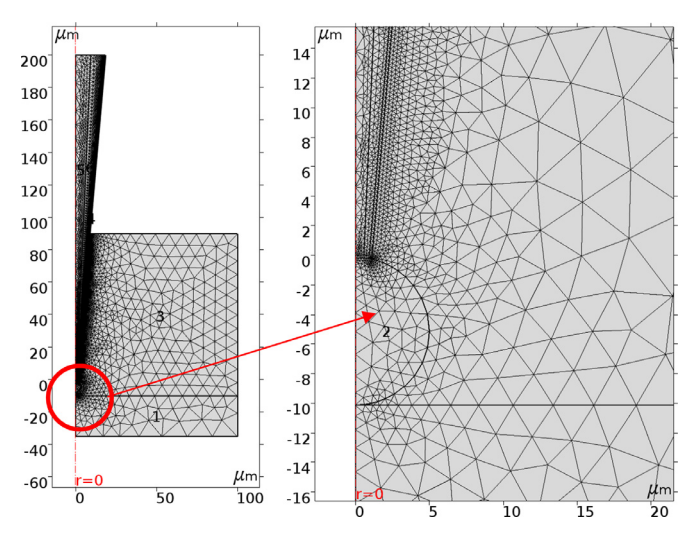


Fig. 5. Free triangular mesh used for the geometry model.

Then the initial conditions for all domain and convective heat flux boundary conditions were set to room temperature of 21 °C. The geometry was meshed using the free triangular mesh element as shown in Fig. 5. The finer mesh was used for the sensor tip and the cell where the temperature change was expected to be significant due to the heat source; normal mesh was used for GM and polyHEMA to save computation time. The complete mesh consisted of 16,042 domain elements and 1,816 boundary elements.

The final mesh for the model was chosen after the mesh sensitivity test, which was completed by refining the mesh until the results did not change between consecutive simulations. For the time-dependent study, the time step was chosen according to the data recording interval in the oscilloscope and the simulation was run for the total time duration of 500 µs, which was the time the laser was irradiated at the sensor tip. The post-processing of the result and data analysis was performed followed by the MATLAB fitting to determine the thermal conductivity of the microspheres and cell.

4. Results and discussions

Our earlier work successfully demonstrated the Micro-Pipette Thermal Sensor (MPTS) technique for the measurement of the thermal conductivity of thin-film samples [32] and fluid samples [31]. We have elaborated on this body of work by measuring the thermal conductivity of an individual biological cell. To validate the MPTS method for measuring the thermal conductivity of spherical samples, the thermal conductivities of three different sized polyethylene microspheres as shown in Fig. 6 were measured.

The three parameters: thermal conductivity, power absorbed, and the radial distance determined by the MPTS technique using multi-parameter fitting are tabulated in Table 1. The optimization with multi-parameter fitting to determine the optimal parameters was repeated for at least three times producing the result with a standard deviation of approximately 2% for all measurements. Therefore, we considered that the MPTS method can generate results with reproducibility of 98%. The measured thermal conductivities for all three sizes did not vary significantly and the averaged value of $0.327~\text{W/(m\cdot K)}$ deviated from the literature value by only 0.8%. Hence, the accuracy of the thermal conductivity measurement for the spherical sample using the MPTS technique can be considered to have an error of less than 1%.

After validating the MPTS technique by measuring the thermal conductivity of the polyethylene microsphere, the method was used to measure the thermal conductivity of three different Jurkat

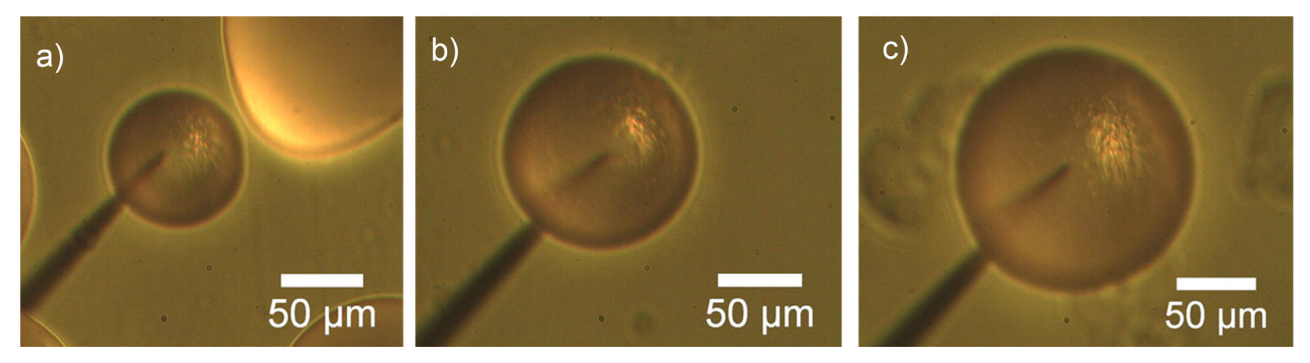


Fig. 6. Thermal conductivity measurement using MPTS on 3 different sized polyethylene microspheres. a) microsphere with $r = 39.7 \mu m$, b) microsphere with $r = 74.5 \mu m$.

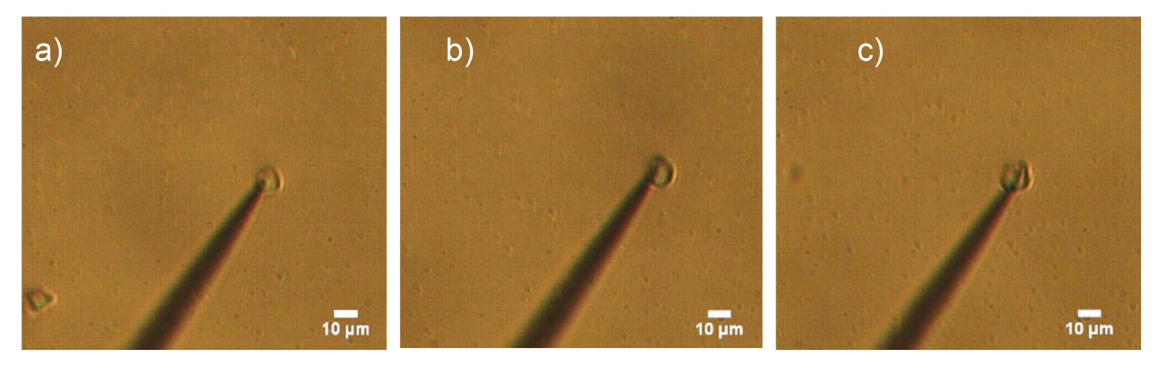


Fig. 7. Thermal conductivity measurement using MPTS on 3 different Jurkat cells.

Table 1Thermal conductivities of microsphere and Jurkat cell.

SN	Test Samples	Experiment	Literature			
		Thermal Conductivity (W/m.K)	Optimized Radial Distance (μ m)	Power Absorbed (µW)	Thermal Conductivity (W/m.K)	
1	Microsphere 1	0.324 ± 2.2%	6.25	109.02	0.33	
2	Microsphere 2	$0.317\pm2.3\%$	5.90	104.33		
3	Microsphere 3	$0.341 \pm 1.4\%$	6.24	109.03		
4	Jurkat Cell 1	$0.534 \pm 1.2\%$	5.00	81.19	NA	
5	Jurkat Cell 2	$0.544 \pm 1.9\%$	4.83	81.94		
6	Jurkat Cell 3	$0.537 \pm 1.6\%$	5.05	81.86		

cells extracted from the culture growing in the doubling phase. The images captured during the measurement process when the sensor was positioned on the cell surface are shown in Fig. 7.

Using the Imagel software, the average diameter of the cells used for the experiment was found to be 10.5 µm with a standard deviation of 1.6 µm. Three single cells selected to measure the thermal conductivity as shown in Fig. 7 were measured to have a diameter of a) 10.4 µm, b) 11.7 µm and c) 12.7 µm. For the experiment, 30-50 µl of cell suspension was pipetted on the polyHEMA surface and the cells could settle down. The volume was found to be sufficient to cover the chamber surface dispersing the cells on top of polyHEMA. However, the height of GM on top of the surface was difficult to measure accurately. Therefore, a parametric study was conducted with COMSOL simulation to determine the effect of the height of GM on the polyHEMA surface and the cell. The solution was obtained for the liquid height of 1–100 μm with an increment of 10 µm. It was observed that the liquid height of more than 30 µm was required so that there would be no significant effect due to the boundary at room temperature of 21 °C.

Therefore, during the experiment, the sensor was immersed into the GM at a depth $>50~\mu m$ which was confirmed by measuring the sensor leg as shown in Fig. 8 (c). Whenever the sensor touched the surface of the GM, a dark spot could be seen in the real-time image captured by the camera; this dark spot was used

as the reference point to measure the distance to the tip (I). The depth (h) to which the sensor was immersed was calculated using $h=1 \sin{(45^{\circ})}$ which was found to be greater than 70 μ m for the image shown in Fig. 8 (c). Then the measurement of the temperature by MPTS was conducted for three Jurkat cells at room temperature of 21 °C and the multi-parameter fitting process was repeated at least 3 times for each cell to determine the thermal conductivity.

The thermal conductivity determined by the MPTS method for each cell is listed in Table 1. As there was no significant variance in all three thermal conductivity measurements, we averaged the value and report that the thermal conductivity of the live Jurkat cell to be 0.538 W/(m·K) \pm 1%. This value was found to be 90% of the thermal conductivity of water which is the major constituent in the live cell.

The second and third parameters, the radial distance where the temperature is measured, and the power absorbed at the sensor tip, used for the optimization and fitting, were also in good agreement with the theory of heat conduction. The higher power absorption in the microsphere measurement was accounted for by the lower loss when the sensor was in the air compared to the cell measurement in GM. The radial distance was correlated to the thermal penetration depth of the specific material. The thermal penetration depth ($\delta = \sqrt{(\alpha t/\pi)}$) calculated for the

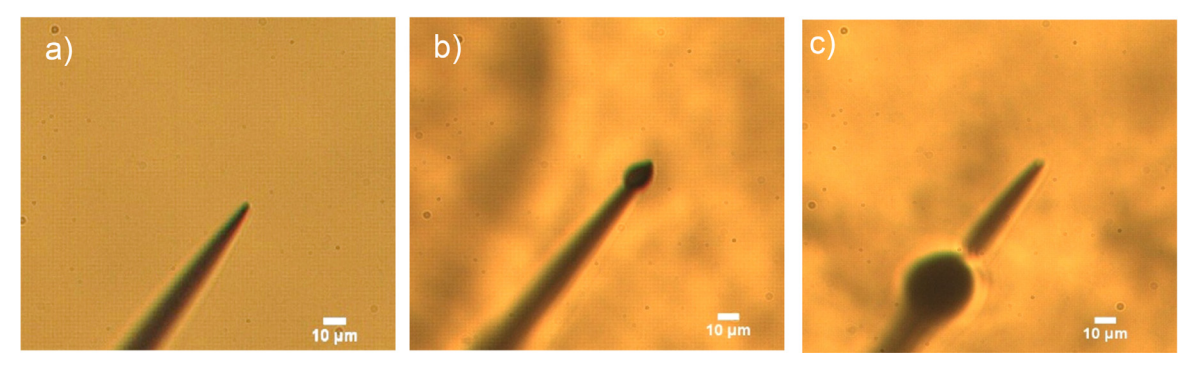


Fig. 8. Manipulation of the sensor to make certain that the sensor tip was immersed at a depth to be considered to have no significant boundary effect. a) sensor in air, b) sensor tip touching the GM surface, c) tip immersed into the GM.

polyethylene microsphere was 5.45 μm and that for Jurkat cell was 4.5 μm , which is a little lower than the measured value by the MPTS technique. The average thermal penetration depth measured for polyethylene microsphere and Jurkat cell were 6.13 μm and 4.96 μm respectively. These are reasonable values if we consider the spatial resolution of the sensor being $\pm 0.81~\mu m$ as the sensor used in the measurement had a diameter of 1.62 μm . Therefore, the radial distance used as the fitting parameter can be correlated to the thermal penetration depth for the test material.

The surface plot for the temperature field with the optimal parameter determined by the MPTS technique and predicted by the COMSOL simulation is shown in Fig. 9. In order to apply the suggested spherical model to biological cells in general, we have generated a non-spherical model and calculated the temporal temperature profile of an ellipsoidal shape. The simulation shows that upon exposure to the sensor tip, the short pulse (500 µs), induces much smaller thermal penetration as compared to the cell size. This implies that provided the sensor touches on the exterior surface of the cell with appropriate contact (detailed procedure of making appropriate contact can be found in Ref. [32]), then regardless of the shape of the cells, the temporal temperature profile, and thus, the thermal conductivity measurement will return the same result as with the spheres; this result will be within reasonable deviation. The temperature profiles obtained from simulation for the spherical and 2 ellipsoidal models are presented in Fig. 9, which show reasonable agreement among them.

The fluorescence image of the experimental cells before and after the temperature measurement with the MPTS, shown in Fig. 10, confirmed that the cells were still viable under the experimental conditions captured as the stress due to sensor positioning and laser irradiation. The change in fluorescence intensity at the end of the experiment could be considered due to the exposure of white light or downstream, potentially repairable, cell effects related to experimental study design. Future experimental study design to understand the degree and duration of the MPTS technique's effect on a biological cell can address fluorescence intensity tracing, structural morphology combined with data acquisition and analysis. Important in our investigation is that the Jurkat cell was still capable of esterase hydrolysis (non-fluorescence calcein conversion to fluorescent calcein) after the sensor measurement method. Therefore, the MPTS technique can be described as a mechanically non-invasive measurement technique that permits maintenance of the tested cell's viability.

Major constituents of cells consist of water, inorganic ions, and organic molecules. Water, which is the most abundant molecule in cells constitutes 70–75% of the total cell mass, inorganic ions account for 1% or less and the remaining are organic compounds [40,41]. The organic compounds in the cells are mainly carbohydrates, lipids, nucleic acids, and proteins out of which proteins con-

stitute 15–20% of total cell mass. Therefore, if we consider the water and protein as the 2 major constituents of the cells that are responsible for the effective thermal conductivity of the cell, we can estimate the composition of the cell by using the effective thermal conductivity model used for heterogeneous material. Even though the suggested effective medium theory model is quite simple and it usually applies to porous media, the purpose of using this model is to support that the measurement of thermal conductivity of a cell can be used to approximate the constituents of a cell. We compared three models: 1) Levy's model, 2) Effective medium theory (EMT) model and 3) combination of Maxwell-Euken (ME1) and EMT model [42,43].

The expression for effective thermal conductivity of the mixture using Levy's mathematical model, which is based on the Maxwell-Eucken model is.

$$K = k_1 \frac{2k_1 + k_2 - 2(k_1 - k_2)A}{2k_1 + k_2 + (k_1 - k_2)A}$$
(3)

where, K= effective thermal conductivity of mixture, k_1 , k_2 = thermal conductivity of components (continuous matrix and disperse) in the mixture and A is expressed as,

$$A = \frac{2/G - 1 + 2\nu_2 - \sqrt{(2/G - 1 + 2\nu_2)^2 - 8\nu_2/G}}{2}$$
 (4)

where, v_2 = volume fraction of disperse in matrix and G is expressed as.

$$G = \frac{(k_1 - k_2)^2}{(k_1 + k_2)^2 + k_1 k_2 / 2} \tag{5}$$

Similarly, EMT model is expressed as:

$$v_1 \frac{k_1 - K}{(k_1 + 2K)} + v_2 \frac{k_2 - K}{(k_2 + 2K)} = 0$$
 (6)

And ME1 model is expressed as:

$$K = \frac{k_1 \nu_1 + k_2 \nu_2 (3k_1/(2k_1 + k_2))}{\nu_1 + \nu_2 (3k_1/(2k_1 + k_2))}$$
(7)

ME1 model considers the homogenous mixture of continuous and disperse phase while the EMT model uses the random distribution of the constituents. With the use of effective thermal conductivity determined by the MPTS technique for the Jurkat cell and the known thermal conductivity values for water (0.6 W/m·K) as the continuous phase and protein (0.27 W/m·K) [2] as the disperse, Eqs. (3)–(7) can be solved for the models that we considered to obtain v_1, v_2 using the MATLAB solver. The weight percent then can be calculated using the density of water (0.998 g/cm³) [39] and protein (1.35 g/cm³) [44], which is tabulated in Table 2.

Table 2 shows that among the three models, the combination of ME1 and EMT provides the closest prediction to the published data

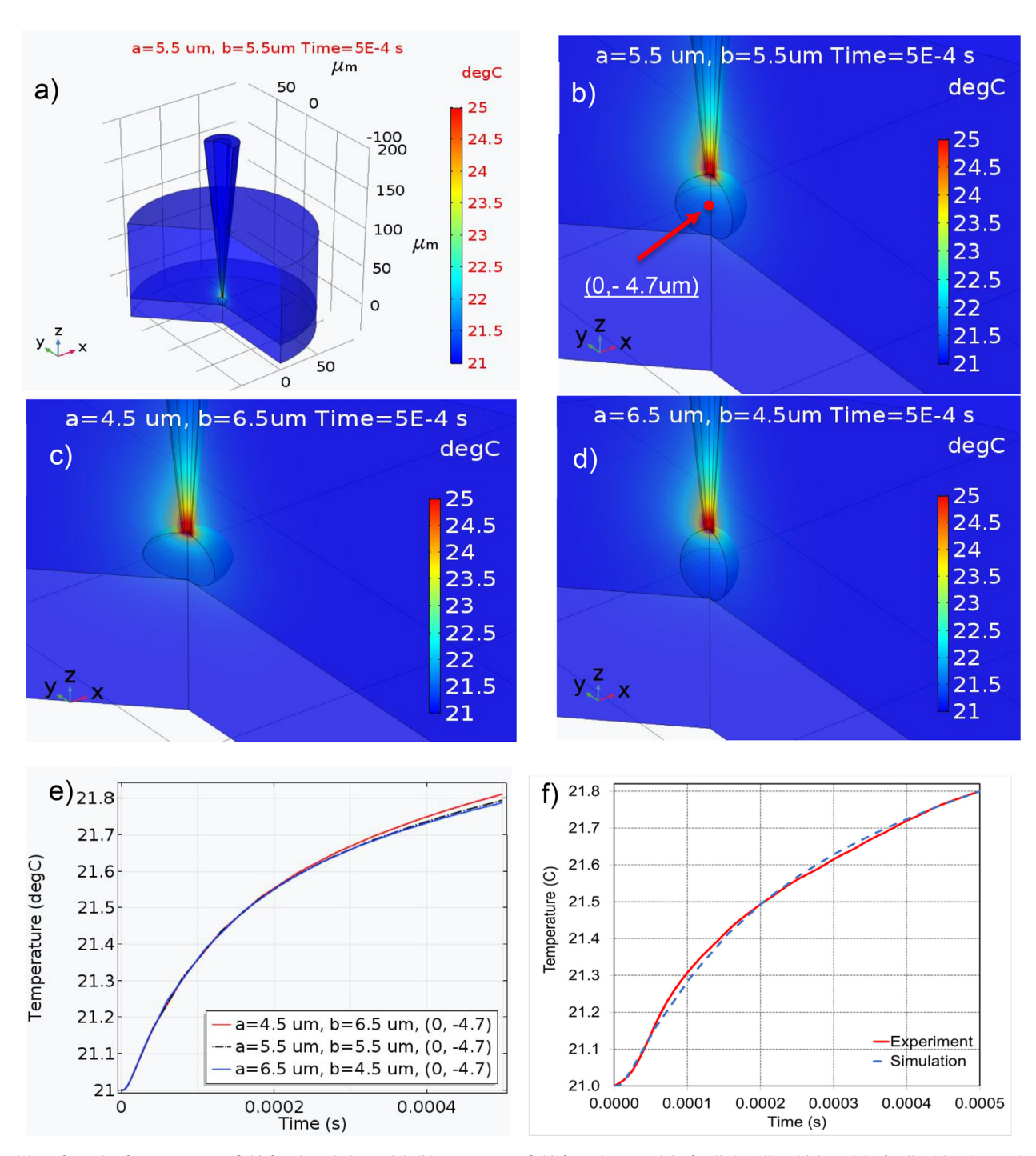


Fig. 9. (a) Surface plot for temperature field for the whole model, (b) temperature field for sphere model of cell, (c) ellipsoidal model of cell with minor axis radius, $a=4.5~\mu m$ and major axis radius, $b=6.5~\mu m$, (d) ellipsoidal model of cell with minor axis radius, $a=6.5~\mu m$ and major axis radius, $b=4.5~\mu m$, (e) line plot for temperature vs time obtained from the simulation for the single-cell on polyHEMA for the 3 different shapes, and (f) fitting of the experimental data and the simulation result with the optimal parameters for the cell.

Table 2Percentage composition of Jurkat cell based on water and protein contents.

SN	Model for Effective Thermal Conductivity	Water Vol. Fraction	Protein Vol. Fraction	Water Wt %	Protein Wt %
1	Levy's	0.8525	0.1475	81.03	18.97
2	EMT	0.8459	0.1541	80.23	19.77
3	ME1+ EMT	0.8279	0.1721	78.05	21.95

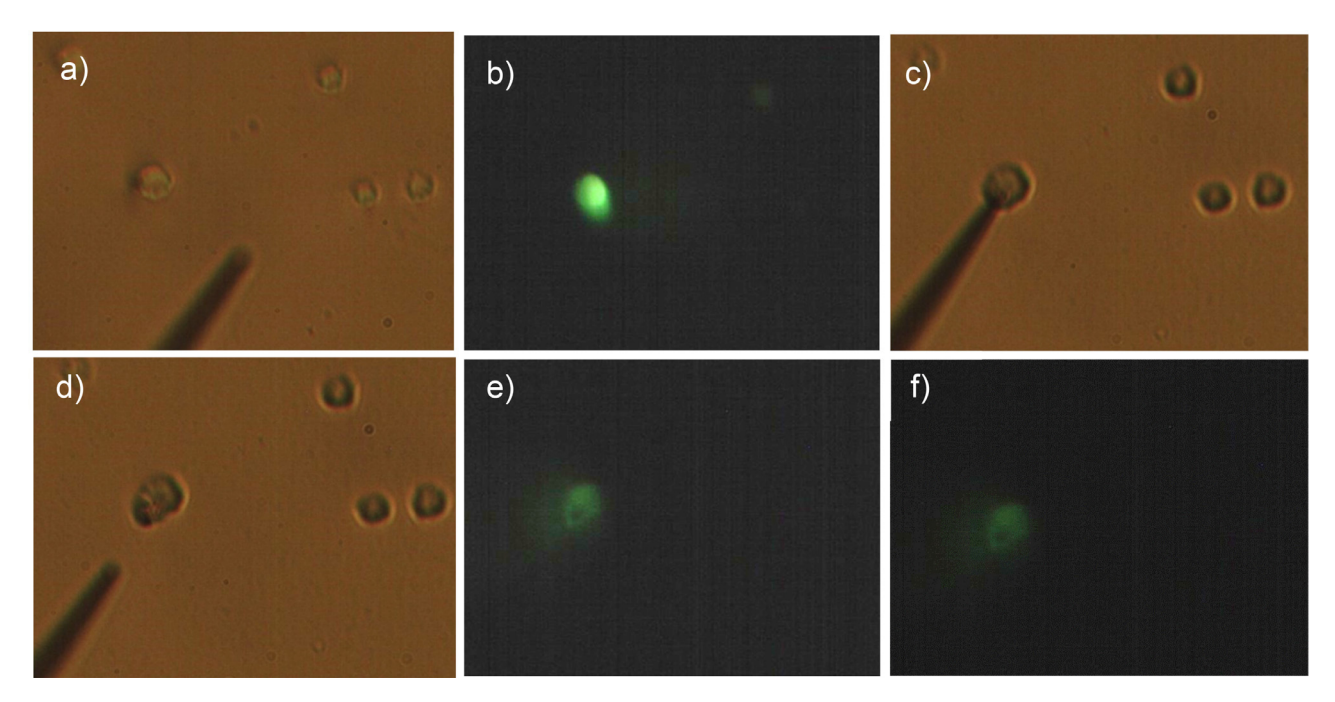


Fig. 10. Fluorescence image for single-cell viability test. a) cell image with white light before the experiment, b) fluorescence image before the experiment, c) positioning of the sensor on cell for measurement, d) removing the sensor from the cell after measurement and e) fluorescence image within 5 min of experiment f) fluorescence image after 15 min of completing the experiment.

(70–75% water and 15–20% protein and remaining other metabolites) [40,41] for the composition of the cell; this is not surprising because this model considers both the part homogeneous and part random distribution of the protein in water, which is more realistic. Therefore, for determining the composition of the cell in terms of water and protein, the combination of ME1 and EMT models is recommended.

5. Conclusions

This work is intended for the development of a characterization technique for measuring the thermal properties of a single biological cell. We demonstrated the validity of the MPTS technique in measuring the spherical microparticles by measuring industrystandard polyethylene microspheres. The thermal conductivity for the microsphere was determined to be 0.327 $W/(m \cdot K)$ by the MPTS technique with reproducibility of 98% and accuracy with less than 1% error, in good agreement with the published data. Finally, the thermal conductivity of the viable Jurkat cell was measured to be 0.538 W/(m·K) \pm 1% which was found to be 90% of the thermal conductivity of the water. The viability of the cell after the measurement technique was confirmed with a calcein-AM fluorescence imaging method. The MPTS method was determined to be a mechanically non-invasive technique as the cells were still capable of esterase hydrolysis reactions and thus viable even after the stress imposed by the sensor, environmental condition, and laser heating during the experiment. We determined that an optimal model predicts a cell's major constituents and address composition influence on effective thermal conductivity combines ME1 and EMT modeling. We, therefore, recommend this combination as the ME1-EMT Model for general use in obtaining the composition of the cell.

We herein conclude that the thermal conductivity measurement using the MPTS is a unique technique for the characterization of thermal properties and temperature measurement of microspheres and single biological cells. Future research could be conducted on measuring the thermal conductivity of a paired normal healthy cell and a diseased cell or transition stages from normal through to disease to determine the differences in thermal properties. These

detectable differences in thermal properties could then be used to improve and to develop clinical applications in diagnosis, screening, treatment

Declaration of Competing Interest

No conflict of interest.

Acknowledgement

This work was supported by National Science Foundation (award number: 1906553).

References

- T.S. Tighe, J.M. Worlock, M.L. Roukes, Direct thermal conductance measurements on suspended monocrystalline nanostructures, Appl. Phys. Lett. 70 (20) (1997) 2687–2689.
- [2] X. Yu, D.M. Leitner, Heat flow in proteins: computation of thermal transport coefficients, J. Chem. Phys. 122 (5) (2005) 054902.
- [3] C. Dames, G. Chen, Theoretical phonon thermal conductivity of Si/Ge superlattice nanowires, J. Appl. Phys. 95 (2) (2004) 682–693.
- [4] A.A. Balandin, S. Ghosh, W. Bao, Superior thermal conductivity of single-layer graphene, Nano Lett. 8 (3) (2008) 902–907.
- [5] E. Pop, D. Mann, Q. Wang, Thermal conductance of an individual single-wall carbon nanotube above room temperature, Nano Lett. 6 (1) (2006) 96–100.
- [6] K.M. McCabe, M. Hernandez, Molecular thermometry, Pediatr. Res. 67 (5) (2010) 469–475.
- [7] K. Okabe, N. Inada, C. Gota, Intracellular temperature mapping with a fluorescent polymeric thermometer and fluorescence lifetime imaging microscopy, Nat. Commun. 3 (1) (2012) 705.
- [8] G.V. Gavriloaia, A. Hurduc, A. Ghimigean, Spatial-temperature high resolution map for early cancer diagnosis, Anonymous SPIE 7171 (2009) 71710W-717108.
- [9] B.K. Park, Y. Woo, D. Jeong, Thermal conductivity of biological cells at cellular level and correlation with disease state, J. Appl. Phys. 119 (22) (2016) 224701.
- [10] B.K. Park, N. Yi, J. Park, Note: development of a microfabricated sensor to measure thermal conductivity of picoliter scale liquid samples, Rev. Sci. Instrum. 83 (10) (2012) 106102.
- [11] B.K. Park, N. Yi, J. Park, Development of a thermal sensor to probe cell viability and concentration in cell suspensions, AIP Adv. 4 (4) (2014) 047120.
- [12] C. Rossmann, D. Haemmerich, Review of temperature dependence of thermal properties, dielectric properties, and perfusion of biological tissues at hyperthermic and ablation temperatures, Crit. Rev. Biomed. Eng. 42 (6) (2014) 467–492.

- [13] M.W. Ashraf, S. Tayyaba, N. Afzulpurkar, Micro Electromechanical Systems (MEMS) based microfluidic devices for biomedical applications, Int. J. Mol. Sci. 12 (6) (2011) 3648–3704.
- [14] S.R. Choi, D. Kim, Measurement of thermal properties of microfluidic samples using laser point heating thermometry, Thermochim. Acta 455 (1) (2007) 11–15.
- [15] L. Shi, A. Majumdar, Thermal transport mechanisms at nanoscale point contacts, J. Heat Transf. 124 (2) (2001) 329–337.
 [16] H. O'Hanley, J. Buongiorno, T. McKrell, Measurement and model validation of
- [16] H. O'Hanley, J. Buongiorno, T. McKrell, Measurement and model validation of nanofluid specific heat capacity with differential scanning calorimetry, Adv. Mech. Eng. 4 (2012) 181079.
- [17] C. Wang, R. Xu, W. Tian, Determining intracellular temperature at single-cell level by a novel thermocouple method, Cell Res. 21 (10) (2011) 1517–1519.
- [18] M.S. Watanabe, N. Kakuta, K. Mabuchi, Micro-thermocouple probe for measurement of cellular thermal responses, in: *IEEE Engineering in Medicine and Biology*, 27th Annual Conference, Anonymous, 2005, pp. 4858-4861.
- [19] G. Fish, O. Bouevitch, S. Kokotov, Ultrafast response micropipette-based submicrometer thermocouple, Rev. Sci. Instrum. 66 (5) (1995) 3300–3306.
- [20] G. Paul, M. Chopkar, I. Manna, Techniques for measuring the thermal conductivity of nanofluids: a review, Renew. Sustain. Energy Rev. 14 (7) (2010) 1913–1924.
- [21] A.S. Ahuja, K.N. Prasad, W.R. Hendee, Thermal conductivity and diffusivity of neuroblastoma tumor, Med. Phys. 5 (5) (1978) 418–421.
- [22] M.L. Denton, M.S. Foltz, G.D. Noojin, Determination of threshold average temperature for cell death in an in vitro retinal model using thermography, Anonymous (2009) 7175.
- [23] Denis de Senneville, B., Quesson B FAU Moonen, C. T. W., and Moonen, C. T., "Magnetic resonance temperature imaging," Int. J. Hyperthermia, North American Hyperthermia Group JID - 8508395.
- [24] A. WHITE, Effect of pH on fluorescence of tryosine, tryptophan and related compounds, Biochem. J. 71 (2) (1959) 217–220.
- [25] P.K. Chowdhury, K.D. Ashby, A. Datta, Effect of pH on the fluorescence and absorption spectra of hypericin in reverse micelles, Photochem. Photobiol. 72 (5) (2000) 612–618.
- [26] C. Gota, K. Okabe, T. Funatsu, Hydrophilic fluorescent nanogel thermometer for intracellular thermometry, J. Am. Chem. Soc. 131 (8) (2009) 2766–2767.
- [27] J. Yang, H. Yang, L. Lin, Quantum dot nano thermometers reveal heterogeneous local thermogenesis in living cells, ACS Nano 5 (6) (2011) 5067–5071.
- [28] F. Vetrone, R. Naccache, A. Zamarrón, Temperature sensing using fluorescent nanothermometers, ACS Nano 4 (6) (2010) 3254–3258.

- [29] L. Gao, L. Wang, C. Li, Single-cell photoacoustic thermometry, J. Biomed. Opt. 18 (2) (2013) 26003.
- [30] G. Kucsko, P.C. Maurer, N.Y. Yao, Nanometre-scale thermometry in a living cell, Nature 500 (7460) (2013) 54–58.
- [31] R. Shrestha, R. Atluri, D.P. Simmons, A micro-pipette thermal sensing technique for measuring the thermal conductivity of non-volatile fluids, Rev. Sci. Instrum. 89 (11) (2018) 114902.
- [32] R. Shrestha, K.M. Lee, W.S. Chang, Steady heat conduction-based thermal conductivity measurement of single walled carbon nanotubes thin film using a micropipette thermal sensor. Rev. Sci. Instrum. 84 (3) (2013) 034901.
- [33] R. Shrestha, T. Choi, W. Chang, A high-precision micropipette sensor for cellular-level real-time thermal characterization, Sensors 11 (9) (2011) 8826–8835
- [34] H.S. Carslaw, J.C. Jaeger, in: Conduction of heat in solids, second ed., Clarendon Press, Oxford. 1959. p. 255.
- [35] J. Myungjin Lee, P. Mhawech-Fauceglia, N. Lee, A three-dimensional microenvironment alters protein expression and chemosensitivity of epithelial ovarian cancer cells in vitro, Lab. Investig. 93 (2013) 528.
- [36] S.H. Tan, N. Nguyen, Y.C. Chua, Oxygen plasma treatment for reducing hydrophobicity of a sealed polydimethylsiloxane microchannel, Biomicrofluidics 4 (3) (2010) 032204.
- [37] T. Adam, T.S. Dhahi, U. Hashim, Fabrication of PDMS microfluidic via room temperature rapid prototyping process, Adv. Mater. Res. 1109 (2015) 340– 344.
- [38] X. Hun, Z. Zhang, Preparation of a novel fluorescence nanosensor based on calcein-doped silica nanoparticles, and its application to the determination of calcium in blood serum, Microchim. Acta 159 (3) (2007) 255–261.
- [39] D.R. Lide, in: CRC Handbook of Chemistry and Physics, 85th ed., CRC Press, Boca Raton, FL, 2005, pp. 3–6.
- [40] Cooper, J. A., Lodish, H. F., Chow, C., Bernfield, M. R., 2019, "Cell," Retrieved from https://www.britannica.com/science/cell-biology.
- [41] G.M. Cooper, The Cell: a Molecular Approach, second ed., Sinauer Associates, Sunderland, MA, 2000.
- [42] J.K. Carson, J. Wang, M.F. North, Effective thermal conductivity prediction of foods using composition and temperature data, J. Food Eng. 175 (2016) 65–73.
- [43] J. Wang, J.K. Carson, M.F. North, A new approach to modelling the effective thermal conductivity of heterogeneous materials, Int. J. Heat Mass Transf. 49 (17) (2006) 3075–3083.
- [44] H. Fischer, I. Polikarpov, A.F. Craievich, Average protein density is a molecular-weight-dependent function, Protein Sci. 13 (10) (2004) 2825–2828.